Supplemental Information

Cytoplasmic dynein transports axonal microtubules in a polarity-sorting manner

Anand N. Rao[1], Ankita Patil[1], Mark M. Black[2], Erin M. Craig[3], Kenneth A. Myers[4], Howard T. Yeung[3], and Peter W. Baas[1,5]

[1]Department of Neurobiology and Anatomy, Drexel University, Philadelphia, PA 19129

[2]Department of Anatomy and Cell Biology, Temple University, Philadelphia, PA 19140

[3]Department of Physics, Central Washington University, Ellensburg, WA 98926

[4]Department Biological Sciences, University of the Sciences, Philadelphia, PA 19104

Abbreviations: Microtubule (MT)

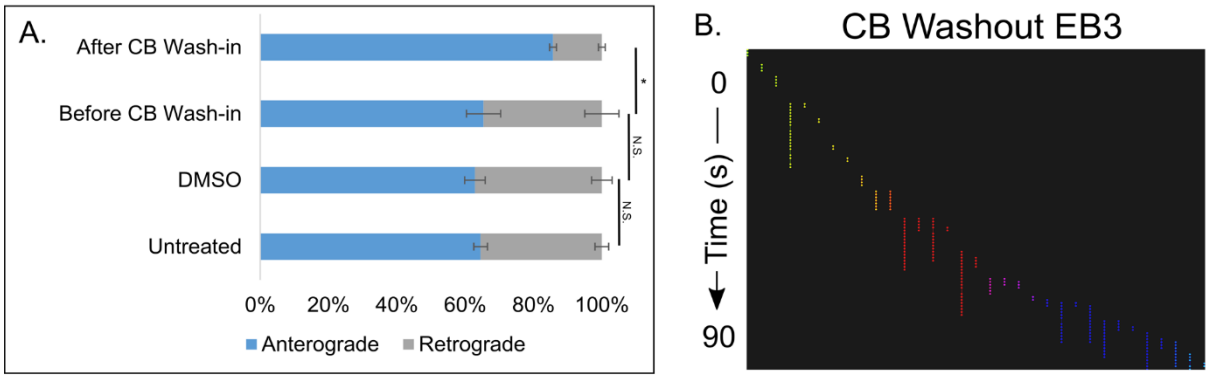

Figure S1 – **CB preferentially affects vesicle transport directionality and does not affect EB3 run length after washout (related to Figure 1 and 2)**

A. Bar graph showing preferential inhibition of retrograde transport directionality of membranous vesicles with CB or vehicle. **B.** Track plot of EB3 comets over 90 s after CB washout. Each colored track represents an EB3 comet and the track length plots the time of the comet run. No significant difference was found across treatments. n=25 neurons per condition from 3 independent dissections. * - $p<0.05$; N.S. = no significance

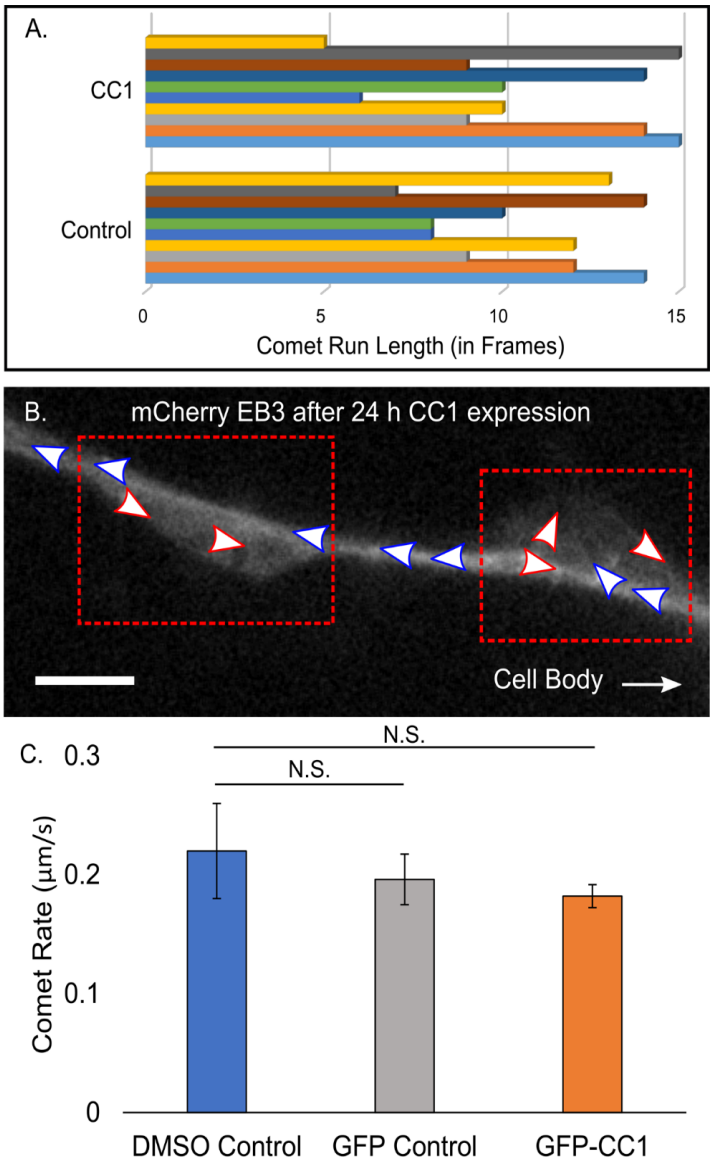

Figure S2 – **CC1 expression does not affect EB3 run length but creates pockets of polarity flaws (related to Figure 2)**

A. Bar graph displaying comet run length after expression of an empty GFP construct or GFP-CC1 expression. No significant difference was observed between treatments. **B.** Representative image of an axon showing regions of mal-oriented MTs. For clarity, arrowheads were superimposed on EB3 comets, indicating plus-end-out MTs (blue arrowheads) or minus-end-out MTs (red arrowheads). **C.** Bar graph depicting comet rate after DMSO, expression of an empty GFP construct or GFP-CC1 expression. No significant difference was detected among treatments. Scale bar, 10 µm. n=25 neurons per condition from 3 independent dissections. N.S. = no significance

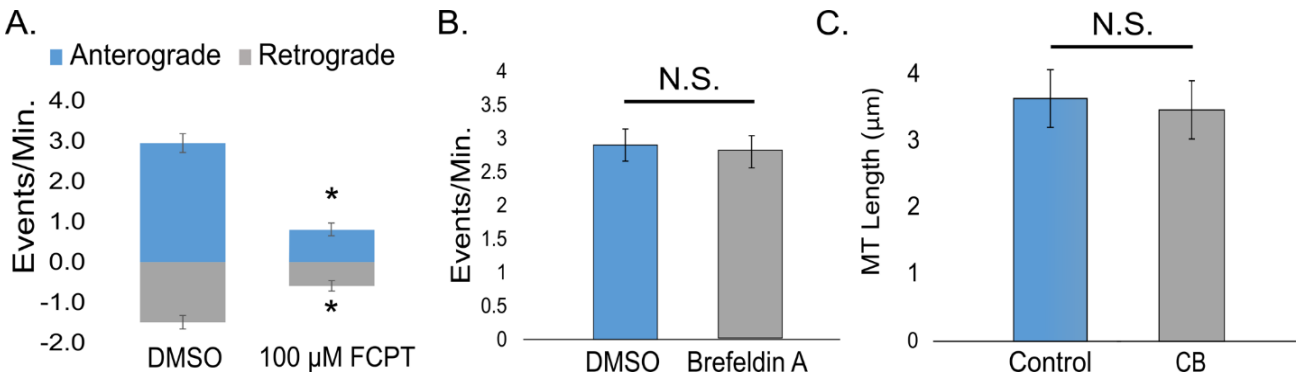

Figure S3 – **MT transport is disrupted by FCPT but not Brefeldin A and MT length is not affected by CB (related to Figure 3)**

A. Bar graph of MT transport in axons of neurons treated with vehicle or FCPT (100 µM). **B.** Bar graph of MT transport in axons of neurons treated with vehicle or Brefeldin A (1 µg/mL). **C.** Bar graph depicting the average length of MTs transported in the axon. n=25 neurons per condition from 3 independent dissections. * - $p<0.05$; N.S. = no significance

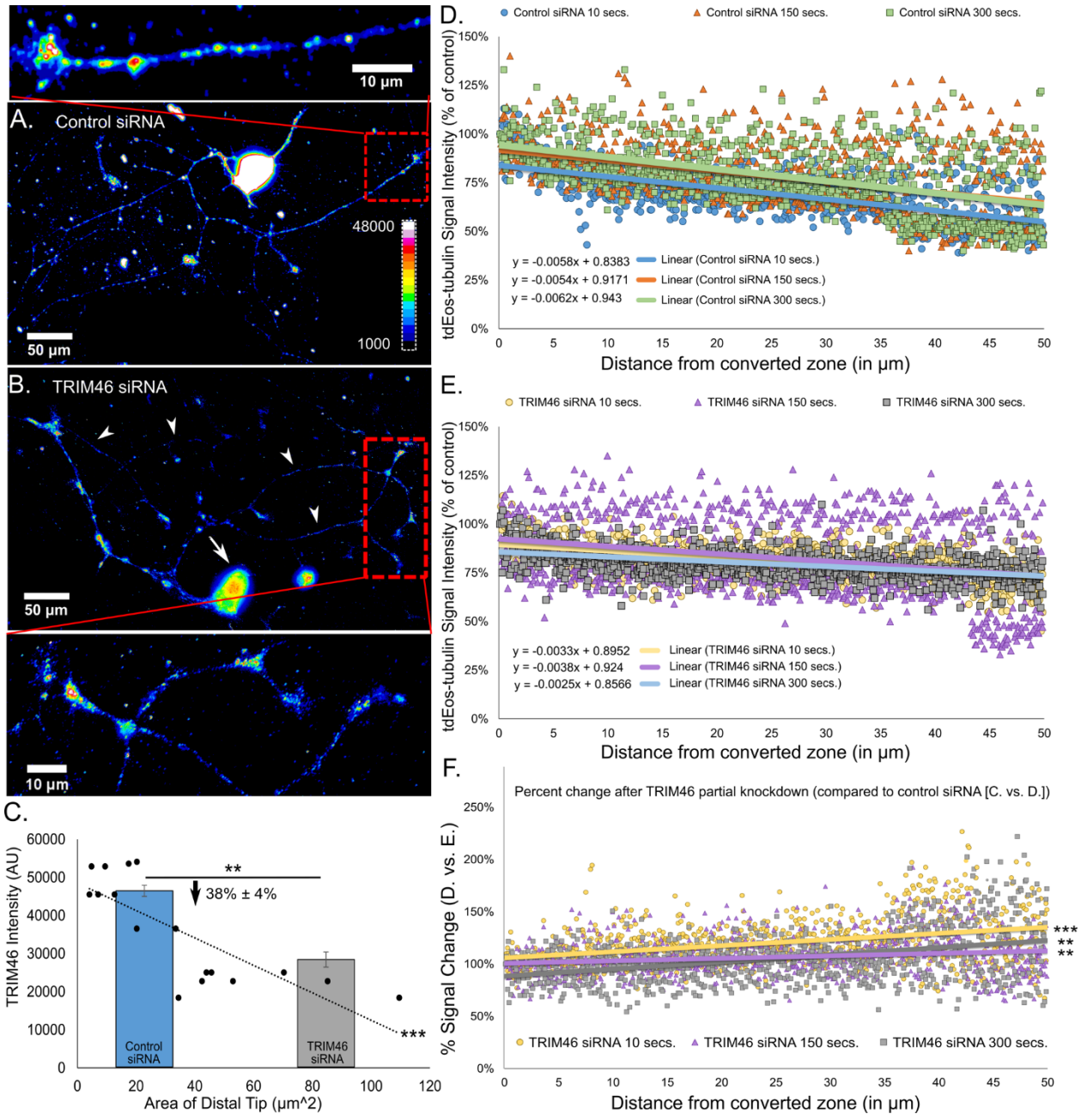

Figure S4 – **TRIM46 siRNA partial depletion results in altered MT transport in the axon (related to Figure 5)** **A. and B.** TRIM46 immunostaining (shown in FIJI "16 color" LUT) of SCG neurons after treatment with control (upper) or TRIM46 (lower) siRNA. **C.** Combined bar graph depicting protein levels after treatment, and scatter plot depicting the correlation between TRIM46 signal and the area of the distal tip (morphological measurement). **D.** Scatter plot showing tdEos-tubulin signal (y-axis) over distance from converted zone (x-axis) after treatment with control siRNA. tdEos-tubulin signal (i.e., the red signal produced after conversion from green to red) is represented

as a percent of converted zone intensity. Lines of regression and equations are shown below scatter plot. **E.** Scatter plot showing tdEos-tubulin signal vs. distance from converted zone after treatment with TRIM46 siRNA. **F.** Scatter plot representing the percent change in signal intensity after treatment with TRIM46 siRNA when compared with control siRNA treatment at 10 sec, 150 sec, and 300 sec. (178 intensity measurements across 50 microns taken from 15 cells per condition). * - $p<0.05$; ** - $p<0.01$; *** - $p<0.001$

Parameter	Meaning	Value	Reference
ξ	Viscous drag coefficient per unit length for longitudinal free diffusion of a MT	$0.00144\frac{pNs}{\mu m^2}$	Imafuku et al., 1996
γ	Effective viscous drag coefficient per attached cross-linker	$10^3\frac{pNs}{\mu m}$	Pringle et al., 2013 *(We used measurements for MAP65 for an order-of-magnitude estimate of the mechanical features of the static cross-linker proposed in this model.)*
λ	Maximum linear density of motor attachment to MT	$125\mu m^{-1}$	Song et al., 1993.
d_{off}	Cytoplasmic dynein unbinding rate under zero load	$0.37s^{-1}$	Kunwar et al., 2013
k_{off}	Kinesin-1 unbinding rate under zero load	$0.35s^{-1}$	Kunwar et al., 2013
F_{dd}	Cytoplasmic dynein detachment force	$1.74pN$	Kunwar et al., 2013
F_{dk}	Kinesin-1 detachment force	$2.0pN$	Kunwar et al., 2013
F_{sd}	Cytoplasmic dynein stall force	$2.5pN$	Kunwar et al., 2013
F_{sk}	Kinesin-1 stall force	$2.5pN$	Kunwar et al., 2013
v_{bd}	Characteristic velocity parameter for cytoplasmic dynein under super-stall loads	$0.001\frac{\mu m}{s}$	Kunwar et al., 2013
v_{bk}	Characteristic velocity parameter for kinesin-1 under super-stall loads	$0.001\frac{\mu m}{s}$	Kunwar et al., 2013
v_{fd}	Cytoplasmic dynein velocity under zero load	$3.5\mu m$	Ahmad et al., 2006 (Parameter tuned to match velocity histograms of short axonal MTs in Ahmad et al., 2006).
v_{fk}	Kinesin-1 velocity under zero load	$1.0\mu m$	Ahmad et al., 2006

Supplemental Table 1 – Input parameters used in simulations, constrained based on experimental measurements (related to Figure 4).

Experimental Procedures

Antibodies and Reagents: *Drug treatments:* Ciliobrevin D (Calbiochem; Cat. # 250401) was dissolved in DMSO (Culture grade; Sigma) at concentrations of 50 and 100 μM, which have been shown to inhibit dynein (Firestone et al., 2012). FCPT (gift from Dr. Timothy Mitchison) was dissolved in DMSO (Sigma) at a concentration of 50 μM, which has been shown to prevent MT transport (Rao et al., 2016). An equivalent volume of DMSO alone was used for vehicle control treatments. *Antibodies:* β3-tubulin (Biolegend; Cat.# 801202); actin (Molecular Probe; Cat.# A12379); anti-Golgi 58k antibody (abcam cat. # ab27043); TRIM46 (Santa Cruz; Cat.# sc-104716). *TRIM46 siRNA:* Sigma TRIM46 (rat) 1. SASI_RN02_00231325; 2. SASI_RN02_00231326; 3. SASI_RN02_00231327; 4. SASI_RN02_00231328.

Computational Modeling: Following the mean-field approach of (Muller et al., 2008), a linear force-velocity curve for individual motors was used:

$$v(F) = \begin{cases} v_F\left(1 - \dfrac{F}{F_s}\right) & for\ F \le F_s \\ v_B\left(1 - \dfrac{F}{F_s}\right) & for\ F \ge F_s \end{cases} \quad (1)$$

Values of v_F, v_B, and F_s for kinesin and dynein, based on experiments and previous models, are summarized in Supplemental Table 1. These values were used unless otherwise specified. The number of engaged dynein motors, N_d, is given by:

$$\frac{dN_d}{dt} = r_{d,on} - r_{d,off}N_d \quad (2)$$

where

$$r_{d,on} = d_{on}(N_{tot} - N_d - N_k - N_x) \quad (3)$$

and

$$r_{d,off} = \varepsilon_d \Omega_d(F) + \frac{2v}{L} \quad (4)$$

The parameter d_{on} describes the rate of dynein attachment per available binding site, and the total number of binding sites on the MT, N_{tot}, is proportional to MT length. The first term of equation (4) characterizes the force-dependence of the motor detachment probability. Based on experimental measurements in (Kunwar et al., 2011), for dynein the functional form was used:

$$\Omega_d(F) = \begin{cases} exp\left(\frac{F}{F_d}\right) & F < F_s \\ \frac{1}{0.25*\left(1-exp\left(\frac{-F}{1.97}\right)\right)} & F \geq F_s \end{cases} \quad (5)$$

The second term in equation (4) accounts for the increased motor detachment rate due to the MT sliding past immobilized motors. Equations of the same form as equations (2-4) are used to describe kinesin attachment and detachment kinetics, but with the detachment function measured in (Kunwar et al., 2011) for kinesin:

$$\Omega_k(F) = \begin{cases} exp\left(\frac{F}{F_d}\right) & F < F_s \\ 1.54 + 0.19 * F & F \geq F_s \end{cases} \quad (6)$$

Static cross-linkers were assumed to attach with a rate x_{on}, and detach with a rate x_{off}, and attached cross-linkers opposes MT motion with protein friction given by $N_x \gamma v$, where N_x is the number of engaged cross-linkers, γ is a viscous drag coefficient, and v is the MT transport velocity. In each time step of the simulation, the MT velocity was determined by the over-damped motion condition that the total forces on the MT are balanced, and the condition that all the engaged motors move at the same velocity consistent with their load-velocity characteristics. In the event that multiple motors of the same polarity are simultaneously attached to the MT, they share the load force equally. In this study, the role of each of the major components in the model (dynein, kinesin, and cross-linkers) was explored by

tuning their attachment rates (d_{on}, k_{on}, and x_{on}, respectively) while setting other parameters to realistic values and keeping them constant. For dynein: v_F = 3.5μm/s, v_B = 0.001μm/s, F_s = 2.5pN, and F_d =1.7pN. For kinesin-1: v_F = 2.0μm/s, v_B = 0.001μm/s, F_s = 2.5pN, and F_d = 2.0pN. For the hypothetical cross-linkers, the effective viscous drag coefficient per cross-linker was set to $\gamma = 10^3 \frac{pNs}{\mu m}$.

DHC siRNA and CC1 expression: Four different siRNA duplexes were designed against different regions of the DHC sequence using Dharmacon's custom SMARTpool siRNA service (rat cytoplasmic DHC1; GenBank/EMBL/DDBJ accession no. NM_019226): 5'-gggaggaggttatgtttaa-3', 5'-ggtgacagctttcgaatga-3', 5'-ccaaatacctacattactt-3', and 5'-gctcaaacatgacagaatt-3'. The siRNAs targeting DHC were also used individually to confirm specificity. Data presented were generated from cells treated with pooled siRNAs. The nonspecific duplex III (Dharmacon) was used as control. GFP-CC1 was a gift from Dr. Erika Holzbaur. GFP-CC1 and mCherry-EB3 were co-expressed by nucleofection (Amaxa Nucleofector II™) in SCG neurons and imaged 24h post-transfection.

Supplemental References

FIRESTONE, A. J., WEINGER, J. S., MALDONADO, M., BARLAN, K., LANGSTON, L. D., O'DONNELL, M., GELFAND, V. I., KAPOOR, T. M. & CHEN, J. K. 2012. Small-molecule inhibitors of the AAA+ ATPase motor cytoplasmic dynein. *Nature,* 484**,** 125-9.

KUNWAR, A., TRIPATHY, S. K., XU, J., MATTSON, M. K., ANAND, P., SIGUA, R., VERSHININ, M., MCKENNEY, R. J., YU, C. C., MOGILNER, A. & GROSS, S. P. 2011. Mechanical stochastic tug-of-war models cannot explain bidirectional lipid-droplet transport. *Proc Natl Acad Sci U S A,* 108**,** 18960-5.

MULLER, M. J., KLUMPP, S. & LIPOWSKY, R. 2008. Tug-of-war as a cooperative mechanism for bidirectional cargo transport by molecular motors. *Proc Natl Acad Sci U S A,* 105**,** 4609-14.

RAO, A. N., FALNIKAR, A., O'TOOLE, E. T., MORPHEW, M. K., HOENGER, A., DAVIDSON, M. W., YUAN, X. & BAAS, P. W. 2016. Sliding of centrosome-unattached microtubules defines key features of neuronal phenotype. *J Cell Biol,* 213**,** 329-41.